A High Resolving Power Ion Selector for Post-source Decay Measurements in a Reflecting Time-of-flight Mass Spectrometer

C. K. G. Piyadasa[1]*, P. Håkansson[2], T. R. Ariyaratne[1] and D. F. Barofsky[3]

[1]Department of Physics, University of Colombo, Colombo-03, Sri Lanka
[2]Division of Ion Physics, Ångström Laboratory, Box 534, S-751 21 Uppsala, Sweden
[3]Department of Chemistry, 153 Gilbert Hall, Oregon State University, Corvallis, Oregon 97331-4003, USA

SPONSOR REFEREE: W. Ens, Physics Dept., University of Manitoba, Winnipeg, Canada

An electrostatic deflector has been designed and constructed that can be used in a reflecting time-of-flight mass spectrometer for either single-deflector or dual-deflector velocity selection in post-source decay measurements. The deflector consists of an interleaved set of parallel deflection electrodes as in a Loeb/Cravath/Bradbury device, but thin metal ribbon instead of wire is used for the deflection electrodes. The time for reversing the electric field, which depends on various factors such as the electronics for pulsing the voltage and the time constant of a particular electrode geometry, is about 19 ns for the deflectors used in this study. By properly timing the reversal of the electric field, the time-window for ion transmission can be made substantially less than the switching time of each individual deflector. In conjunction with matrix-assisted laser desorption/ionization, the single-deflector's resolving power and transmission are robust with respect to laser fluence, i.e. they remain high even when the fluence is raised well above threshold. By contrast the operational features of the dual-deflector gate offer more versatility in locating and sizing the selection window. Operating the ion selector in a single-deflector mode, we have achieved a resolving power of ~710 full width at half maximum (FWHM) for different isotopes of protonated, sodiated, and potassiated substance-P (*m/z* 1348.6, 1370.6 and 1386.6 respectively; 10.073 keV). Operating it in the dual-deflector mode under two different sets of conditions, we have succeeded in obtaining resolving powers of ~1100 (FWHM) for protonated substance-P (*m/z* 1348.6; 10.8 keV) and ~5200 (FWHM) for an isotopomer of PEG 6000 (~*m/z* 6000; 10.04 keV). This accomplishment implies that high-resolution ion selection can be coupled to post-source decay analyses. © 1998 John Wiley & Sons, Ltd.

Since the advent of matrix-assisted laser desorption/ionization (MALDI) mass spectrometry (MS) a decade ago,[1,2] interest in improving the performance and capabilities of time-of-flight (TOF) instrumentation has increased steadily. Attempts to develop tandem (MS/MS) TOF instruments have been particularly keen. The post-source decay (PSD) method introduced by Kaufmann and co-workers[3] has become the most widely used approach to MALDI tandem TOF-MS. Although the technique suffers from many drawbacks, it has made it possible to select peptides from mixtures and partially sequence them using relatively simple, inexpensive instruments. Perhaps most importantly for the long term, PSD analysis has provided much incentive to develop more general and more powerful approaches to tandem TOF-MS.

The simplest way to make MS/MS TOF measurements is to locate a single ion-deflector in the first field-free drift region of a reflector-TOF instrument and use it as MS1 to pick out a precursor ion and the ion-mirror as MS2 to separate the precursor's metastable fragments. This is the technique used in PSD MALDI analyses. By triggering the deflector to turn off and then quickly back on at a precise time following ion extraction from the source, it acts as a gate through which only ions in a narrow velocity range are allowed to pass. For an ion that arrives at the deflector intact from the ion source, the gate functions as a mass filter because the ion's velocity is inversely proportional to the square root of its mass. For an ion or neutral that arrives at the detector as the product of a metastable or induced decomposition, passing through the gate is equivalent to having selected its precursor ion because the velocity of the latter is conserved to the first order in each of its dissociation products (charged or neutral).

To date, either a conventional set of deflection plates[4–10] or a single set of interleaved wire-combs[11–13] has been used in tandem TOF instruments as the MS1 unit. The latter structure was first proposed by Loeb[14] and subsequently constructed and demonstrated as an electron filter by Cravath[15] and by Bradbury.[16] For the purposes of MS/MS of biological molecules, it is only possible to achieve marginally useful mass selectivities with either of these two deflector geometries. LaiHing *et al.* obtained a resolving power of 200 in selecting the metal cluster ion $Pb_{17}{}^+$ (*m/z* 3522, 1700 keV) out of a distribution of clusters containing

*Correspondence to: C. K. G. Piyadasa, Department of Physics, University of Colombo, Colombo-03, Sri Lanka.

from 2 to 20 atoms.[6] Vlasak *et al.* achieved a resolving power of ~170 in isolating diphenylmethane molecular ions (*m/z* 167, 650 eV), and they estimated that a resolving power greater than 300 should be possible by optimizing their device.[13] These resolving powers are among the highest obtained with single deflectors. When kinetic energies equal or exceed 10 keV, which is typically the case in MALDI analyses, the mass selectivities of single-deflector units are substantially poorer than those obtained in these two studies. Judging from published mass spectra[3,12] or comments,[17] resolving powers for selection of PSD precursor-ions near *m/z* 1000 lie between 25 and 125. Limited MS1 mass selectivity of this sort severely restricts the application of tandem TOF mass spectrometers configured with single-deflectors.

The resolving power of MS1 can be increased to unit mass resolution or better at masses and kinetic energies encountered in MALDI analyses if a reflector-TOF mass analyzer[10,18–20] or a double-focusing sector mass analyzer[21–24] is used for the first MS stage. Regrettably, these geometries have low sensitivity because most metastable decay takes place in the first field-free region of MS1 so very few precursor ions survive to the collision cell; moreover, the gas cell interferes with the timing of the MS2 TOF analyzer, thus, further compromising performance.

PSD's simpler approach would clearly be better if the resolving power of the velocity selection could be substantially increased. Cotter has suggested that such improvement is an impossibility because the mass selectivity of an ion-deflection gate placed in the first drift region, no matter how well-designed, would always be limited by the circumstances that (i) mass dispersion is low at this location and (ii) optimum space/time focus is only achieved in the second drift region on the exit-side of an ion reflector.[25] To use a gate to select a band of ions having a single mass from a band characterized by a slightly different mass, the dispersion in time between the two bands at the gate's entrance must be greater than the width of the ions' distribution in time within a band. Cotter's assessment overlooks the possibility that, despite the fact that mass dispersion cannot be increased between ion bands at the point of velocity selection, the time distribution can be substantially decreased by taking advantage of delayed ion extraction[26] to create a space-focal plane exactly at the entrance of the velocity selector and, furthermore, that this focal plane can also be made to coincide with the ion reflector's object plane.

With regard to improving the design of a gating system, Haberland *et al.*[27] and Stoermer *et al.*[28] have independently pointed out that (i) the time resolution of a single-deflector gate is severely limited because a short duration voltage pulse having leading and trailing edges that are both sharp must be used to actuate the gate's shuttering function and (ii) this restriction can be circumvented by sharing the opening and closing actions of the gate between two separate ion deflectors. Haberland and co-workers constructed an ion selector for a tandem TOF instrument out of two sets of conventional deflection plates but determined that the mass selectivity of their device was limited by its size and the relatively slow rise and fall times (30 ns) of their voltage pulsers.[27] Stoermer *et al.* built a gate from two wire-comb deflectors arranged in tandem and driven with 15 ns switches.[28] At 10 keV, this device performed at resolving powers of 280 in isolating isotopomers of $Cs_3Br_2^+$

(*m/z* ~560) and more than 400 in separating isotopomers of Hg_2^+ (*m/z* ~400) — values that are higher than generally obtained with single wire-comb deflectors. Stoermer and co-workers stated that gains in mass selectivity beyond what they achieved by mounting two ion-deflectors in tandem were probably only possible by (i) reducing the fringing fields that extend outside the physical bounds of the deflectors, (ii) using yet faster switches, or (iii) decreasing ion velocity.

Implicit in the view that the resolving power of a deflection gate is ultimately limited by the rate at which it can be opened or shut is the concept that ion selection is a static process in which the electric field strength between the deflection electrodes is strictly zero during the interval selected for ion transmission. It is possible, however, to operate a single-deflector gate or dual-deflector gate in a dynamic, phase-modulated mode that removes the short switching time limitation on resolving power. At the recent ASMS Conference on Mass Spectrometry and Allied Topics in Orlando, Florida, Vestal and co-investigators showed that MS1 resolving powers of the order of 1000 are possible by using delayed ion extraction in combination with two sets of deflection plates operated in a dynamic mode.[29] Independently, we have devised an ion deflector that combines geometrical features taken from both conventional plates and interleaved wire-combs and have used it to experiment with the dynamic ion-selection process in both single-deflector and dual-deflector modes. Compared to any other ion-gating device we are aware of, our assembly has superior operational and analytical characteristics. In this report, we describe its construction, dynamic operating mechanism and performance in our initial tests.

EXPERIMENTAL

Sample preparation

Substance-P (Sigma) was dissolved in distilled water/0.1% TFA to a concentration of about 10^{-5} M. Small amounts of NaCl and KCl were added to this solution to generate $[M + Na]^+$ and $[M + K]^+$ signals of approximately the same strength as the $[M + H]^+$ signal. PEG 6000 (Kebo Lab) was dissolved in distilled water/0.1% TFA to a concentration of about 10^{-3} M.

Solutions of 20 g/L of α-cyano-4-hydroxycinnamic acid (CHCA, Acros Organics) in acetic acid and of 20 g/L of CHCA in 70% acetonitrile were used as the MALDI matrices. Analyte was applied to the probe by depositing 3–4 μL of the acetic acid matrix solution, allowing it to dry, and then depositing 4 μL of a 1:1 (v/v) mixture of the analyte and the acetonitrile matrix solution. The sample was then left to dry under a gentle stream of air.

Instrumental

All experiments were carried out on a MALDI time-of-flight mass spectrometer home built in Uppsala (Fig. 1). The spectrometer is equipped with a delayed extraction (DE) ion source,[30,31] a single stage electrostatic mirror (300 mm long), and two dual micro channel plate detectors. One detector is located behind the mirror, and the other is mounted in front of the ion source in a manner that allows it to be moved between a position that creates a spectrometer with a short flight tube and one that detects reflected ions.
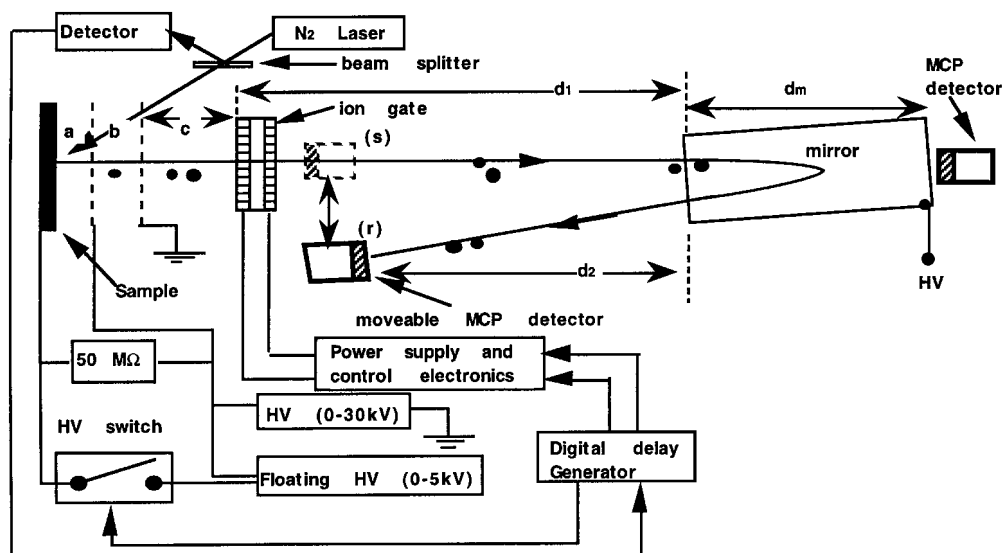
The ion-selector consists of two deflectors mounted in

Figure 1. Diagram of the Uppsala DE MALDI-TOF mass spectrometer. The moveable detector can be placed in position (s) for operating in a short flight tube mode or in position (r) for operating in a reflected mode. Values for the distances indicated in the diagram are as follows: $a = 11.5$ mm, $b = 9.5$ mm, c (L_1 in Eqns (5) and (6)) = 200 mm (for substance-P experiments) and 900 mm (for PEG 6000 experiments), $d_1 = 739$ mm, $d_2 = 440$ mm and $d_m = 300$ mm. The effective distance from the center of the ion-selector assembly to the moveable detector (L_2 in Eqn (6)) ≈ 2100 mm.

tandem. Each deflector is made of 20 parallel lengths of nickel–chromium ribbon (0.09 mm thick × 1.27 mm wide × 15 mm long) spaced 1 mm apart (center to center) to form a venetian blind structure (Fig. 2(a)). In the finished assembly (Fig. 2(b)), the two deflectors are separated by a distance of 10 mm (center to center). These dimensions were chosen to maximize transmission through the ion selector in accordance with SIMION-simulated ion trajectories. The ion selector was located (c in Fig. 1) 200 mm away from the exit grid of the ion source for the experiments
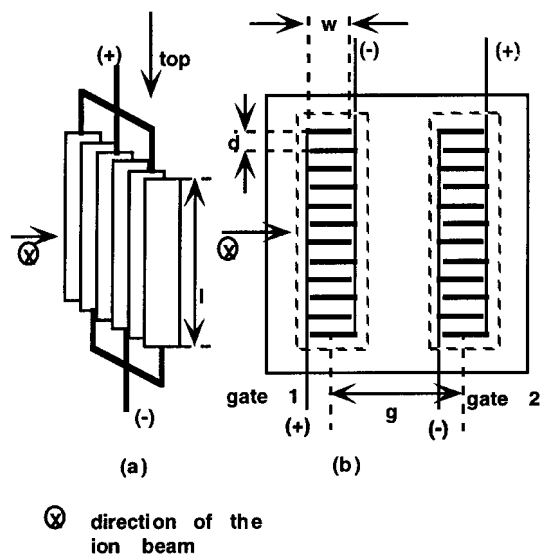
with substance-P and 900 mm away for the experiments with PEG 6000. The distance between the ion selector and the ion mirror (d_1 in Fig. 1) was set so the mirror's object plane would coincide with the ion selector's entrance plane.

To deflect ions, positive and negative potentials of equal magnitude were applied to alternate deflection electrodes as shown in Fig. 2. These voltages were switched on or off with fast high voltage switches (HVS, Behlke HTS 30) controlled by the electronic circuits shown schematically in Fig. 3. The circuit in Fig. 3(a) was used to operate the ion selector in a single-deflector mode, and the modified circuits in Fig. 3(b) were used to drive it in a dual-deflector mode. The front end of the circuit, which is common to both of the configurations, allows the switching phases to be synchronized; this is essential because small variations among the electronic components and the geometries of the interleaved deflection strips would otherwise introduce slight differences in propagation times. A digital delay generator (Stanford Research Institute Model 535) was used to time the triggering pulses for both delayed ion extraction and ion selection.

In operation, the ion-extraction potentials and timing delay were adjusted to make the DE space-focusing plane coincide with the entrance plane of the gate's first deflector and, thus, also with the ion mirror's object plane. The mirror potential was set at 12.77 kV and 10.678 kV respectively for the substance-P and the PEG 6000 measurements.

RESULTS AND DISCUSSION

As a rule, a set of conventional deflection plates is characterized by a relatively high capacitance and by a relatively high electrostatic deflection sensitivity, which indicates the angular divergence induced per volt applied to the electrodes and is determined by the geometry of construction and placement and by the kinetic energy of the ions. Consequently, passing ions receive a substantial lateral impulse from the deflection plates, but the rise and
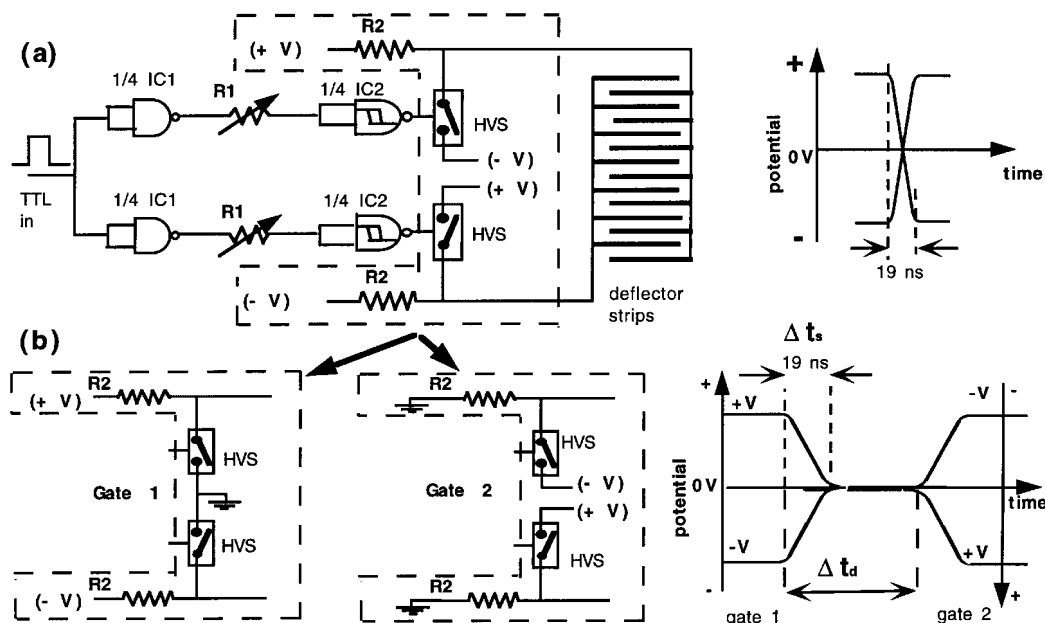

Figure 2. Construction of the dual ion-deflector assembly showing polarities of the potentials applied to the interleaved deflection strips: (a) stereographic view of a single deflector and (b) top view of a dual deflector. The dimensions indicated in the diagram are as follows: l (strip length) = 15.0 mm, strip thickness = 0.09 mm, w (strip width) = 1.27 mm, d (distance between strip centers) = 1.0 mm, and g (distance between deflector centers) = 10.0 mm.

Figure 3. Schematic diagrams of the switching circuits for driving the ion deflectors and the corresponding voltage switching patterns they generate: (a) configuration for single-deflector scanning mode and (b) configuration for dual-deflector scanning mode. The circuits are triggered with TTL pulses originating from a programmable digital delay generator (Fig. 1). The positive and negative voltages ($\pm$ V) applied to the inputs of a high voltage switch (HVS) are produced by a variable, dual-voltage (0–600 V) power supply. The NAND gate (IC1) inverts the TTL trigger pulse and the second NAND gate (IC2) converts the inverted output of IC1 back into a positive TTL pulse. The variable resister R1 provides fine control over the propagation delay of the TTL pulse between IC1 and IC2. A Schmitt triggered NAND gate is used for IC2 to minimize distortion in the TTL pulse delivered to the input of an HVS. The connection between an HVS and a deflector was kept as short as possible in order to minimize the system's capacitance. The deflector geometry and electronic circuitry used in this study produced switching rise and fall times (Δt_s) of 19 ns. The delays in switching times between the two deflectors (Δt_d) were estimated from the mechanical properties of the analytes in accordance with Eqn (3).

fall times of voltage pulses applied to them are severely limited. Just the opposite is the case for an interleaved wire-comb deflector. Our deflector is built in the same way as an interleaved wire-comb, but thin metal-ribbon instead of wire is used for the deflection electrodes. This construction combines the desirable features of both deflection plates and interleaved wire-combs. The venetian blind geometry imparts greater lateral impulse to transiting ions while

Figure 4. Mechanical analogues for different modes of operating ion deflectors: (a–c) single door — hinged, (d–f) single door — revolving, and (g–j) dual door — tandem revolving.

preserving for the most part the low capacitance and, hence, the rapid switching of the wire-comb construction.

The simplest way of selecting a particular ion, the one presently employed in MALDI PSD analyses,[17,31] is by means of a single-deflector operating as illustrated in Fig. 4(a)–(c). In this mode, the gate swings open, like a hinged door, just before the ion band to be selected arrives and closes just after it has passed. The gate's resolution depends for the most part on how rapidly its door can be opened and closed in succession. This is accomplished in practice with an ion deflector by switching the electric field between the electrodes of an electrostatic deflector off and then back on in its original direction. In general, it is difficult to perform these two switching operations in rapid succession because this requires creating a voltage pulse at the deflection electrodes with both sharp rising and falling edges. With present-day electronics, static switching of wire-comb deflectors under MALDI conditions for PSD typically results in resolving powers under 100.[3,12,17]

It is possible to greatly improve the resolution of a single-deflector gate by operating it in the manner depicted in Fig. 4(d)–(f). This revolving door action, which has been described in the past as a means for chopping continuous ion beams into temporally compact ion packets,[32,33] is achieved with an ion deflector by quickly reversing the direction of the electric field between the electrodes in a single switching operation (Fig. 3(a)). As the ion band of interest approaches the gate, its door begins to pivot about its center. The slightly lighter ions arrive at the door before it has rotated very much so they are deflected from their original direction of flight (Fig. 4(d)). If the rate of rotation
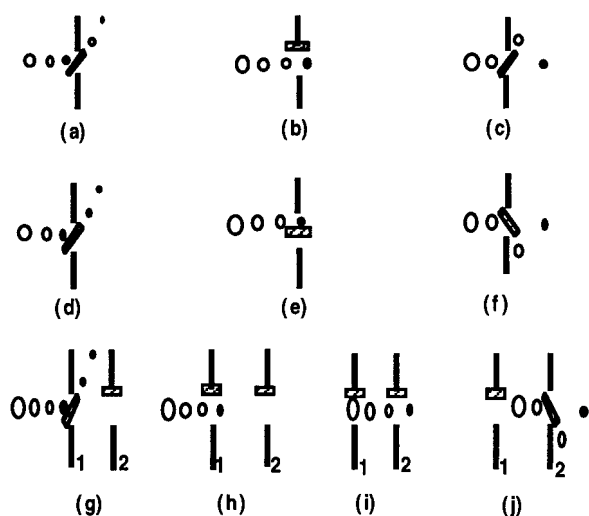
is such that the door just becomes parallel to the flight axis at precisely the moment the ion band to be isolated arrives at its center (Fig. 4(e)), that band can pass through the gate undeflected. The door continues revolving past this open state so that within a very short time it begins to deflect the slightly heavier ions trailing after the selected band (Fig. 4(f)). The duration of the gate's transmission window in this dynamic mode is determined principally by the rate of its door's rotation relative to the speed of the ions.

The revolving door action can also be shared between two doors arranged in tandem as illustrated in Fig. 4(g)–(j). As in the case with one door, the entrance door begins to rotate just as the ions to be selected are about to impinge on it (Fig. 4(g)). When this door reaches its open position however, it locks there so that both the ions of interest and those following closely behind can pass into the space between the two doors (Fig. 4(i)). The second door, which has been held in the open position up to this point, is timed to begin its closing rotation precisely at the moment the desired band of ions pass by its axis of rotation (as a kind of delayed continuation of the first door's motion) so that the door can start deflecting the trailing groups of heavier ions (Fig. 4(j)). When the time between opening door 1 and closing door 2 (Δt_d in Fig. 3(b), is long compared to the times it takes for a door to change its state and for the ions to transit the length of the assembly, the size of the transmission window is determined primarily by Δt_d, and by the speed of the ions — the doors' rates of rotation only play a secondary role. The ion selectivities reported by Haberland et al.[27] and quite recently by Stoermer et al.[28] are characteristic of dual-deflector gates operating in this static shuttering mode. When Δt_d approaches the transit time of a given ion packet, the mechanism for ion selection shifts from a static into a dynamic, phase-modulated mode in which the transmission window is determined mainly by the doors' rates of rotation and the timing between their changes of state in relation to the speed of the ions.

The mechanics of dispersion under phase-modulated conditions can be formally examined by considering the net impulse, $p_x(m)$, delivered to an ion of mass m as it passes through a series of deflectors. By definition this is given by

$$p_x(m) = \int_{t_{entry}(m)}^{t_{exit}(m)} F_x(t)\mathrm{d}t = q \int_{t_{entry}(m)}^{t_{exit}(m)} E_{gate}(t)\mathrm{d}t \quad (1)$$

where $t_{entry}(m)$ is the time an ion effectively enters the ion selector and $t_{exit}(m)$ is the time it effectively exits. This expression will be evaluated initially for the dual-deflector configuration; it will be shown subsequently that the single deflector can be treated as a simple limiting case of the dual deflector. Consider the three, originally axial ions represented in Fig. 5(a) near the entrance to a dual deflector. Just prior to reaching this position, deflector 1 was closed and deflector 2 was open. The situation depicted in Fig. 5(a) occurs just at the time ($t = t_t$) the potential across the plates is triggered to switch off (Fig. 5(d)). Up to this moment, only the lightest ion has experienced an appreciable field, $-2V_{gate}/d$. If the deflector's field collapses in less time, Δt_s, than it takes for the ions to pass through it, the average field strength experienced by the ions during their transit between the first set of plates will vary from roughly $-2V_{gate}/d$ for the lightest ($\Delta m < 0$) to almost zero for the heaviest ($\Delta m > 0$). Consequently, the three ions will be angularly dispersed as depicted in Fig. 5(b).

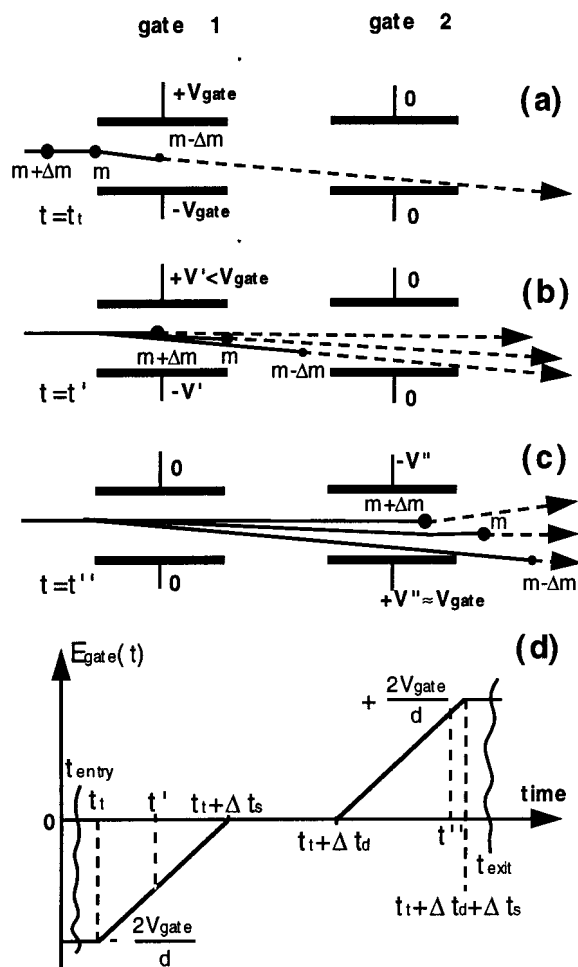Substituting the definition of $E_{dual}(t)$ given in Fig. 5(d)

Figure 5. Principle of dispersing ions in a dual deflector: ion trajectories of ions with masses $m - \Delta m$, m, and $m + \Delta m$ when (a) deflector 1 is triggered to switch off, (b) the electric field in deflector 1 has fallen to approximately half its initial strength, and (c) the electric field in deflector 2 has risen to nearly its full strength. The electric field shown in panel (d) for the dual deflector is given by the following function of time: $E_{dual}(t) \equiv \{-2V_{gate}/d,\ t_{entry} \leq t < t_t;\ (-2V_{gate}/d)[t_t + \Delta t_s - t)/\Delta t_s],\ t_t \leq t < t_t + \Delta t_s;\ 0,\ t_t + \Delta t_s \leq t < t_t + \Delta t_d;\ (+2V_{gate}/d)[(t - t_t - \Delta t_d)/\Delta t_s],\ t_t + \Delta t_d \leq t < t_t + \Delta t_d + \Delta t_s;\ +2V_{gate}/d,\ t_t + \Delta t_d + \Delta t_s \leq t \leq t_{exit}\}$ where d is the distance separating the deflection strips.

into Eqn (1) and evaluating the resulting integrals readily yields the net impulse received by m in this case:

$$p_x(m) = \frac{2q}{d}V_{gate}\{[t_{entry}(m) - t_t] + [t_{exit}(m) - t_t - \Delta t_d - \Delta t_s]\} \quad (2)$$

where t_t is the time at which deflector 1 is triggered to switch off, Δt_s is the switching time for the deflectors (Fig. 3(b)), Δt_d is the delay time between the trigger pulses that switch deflector 1 off and deflector 2 on (Fig. 3(b)), and V_{gate} is the magnitude of the potential applied to the deflection electrodes. In order for m to emerge from deflector 2 moving parallel to the instrument's axis of flight, it must receive an impulse from deflector 2 that exactly cancels the impulse it received from deflector 1 (this zero-net-impulse condition can also be applied to an ion originally traveling at an angle with respect to the flight axis).[32] Imposing this condition on m unambiguously determines the triggering time for the ion selector's first

deflector as a function of m. Substituting $t_{entry}(m) = t_0(m) - \frac{1}{2}t_{transit}(m)$ and $t_{exit}(m) = t_0(m) + \frac{1}{2}t_{transit}(m)$ into Eqn(2), setting $p_x(m) = 0$, and rearranging yields

$$t_{t-dual}(m) = t_0(m) - \frac{\Delta t_d + \Delta t_s}{2} \qquad (3)$$

where $t_0(m) = (L_1 + \frac{1}{2}l_{actual})/v_z(m)$ is m's flight time from the ion source to the halfway point between the ends of the ion selector, $t_{transit}(m) = l_{effective}/v_z(m)$ is m's flight time through the effective length of the ion selector, $v_z(m) = (2qV_{accel}/m)^{\frac{1}{2}}$ is the ion's speed through the selector; $l_{effective} = l_{actual} + l_{fringe}$ is the effective length of the ion selector; l_{actual} is the physical length of the ion-selector; $l_{fringe} \approx d$ is the length added to the ion selector due to fringing fields; and d is the separation between deflection electrodes. For the gate assembly used in this study, $l_{effective} \approx 12.3$ mm (Fig. 2) and $\Delta t_s \approx 19$ ns (Fig. 3). It can be readily seen from Fig. 3 that

$$E_{single-gate}(t) = \lim_{\Delta t_d \to 0} E_{dual-gate}(t).$$

It immediately follows, therefore, that the triggering requirement for a single deflector to select m is given by

$$t_{t-single}(m) = t_0(m) - \frac{\Delta t_s}{2} \qquad (4)$$

Equations (3) and (4) clearly reflect the symmetry of $E_{single}(t)$ and $E_{dual}(t)$ seen in Fig. 3. Although m's final transverse velocity will be zero when either Eqn (3) or (4) is satisfied, its flight path after exiting will be laterally displaced relative to its flight path along the instrument's axis before entering the ion selector.

An ion lighter or heavier than m by an amount Δm will pass through the ion selector slightly out of phase if the deflectors are switched in accordance with Eqn (3) or Eqn (4). Such an ion will experience a net downward ($\Delta m < 0$) or a net upward ($\Delta m > 0$) impulse. Therefore, ions lighter and heavier than m will be angularly dispersed when they emerge from the ion selector; this is depicted in Fig. 5(c) for a dual-deflector arrangement (ions would emerge similarly from a single deflector). If their lateral displacement from the flight axis, $x_{detector}(m + \Delta m)$, is equal or greater than $\frac{1}{2}D_{active}$, when they arrive at the detector plane, they will not be detected. An estimate of $m/\Delta m$ corresponding to this resolution condition can be derived from Eqn (3) assuming (i) all ions are nearly axial and have negligible angular spread so that $D_{effective} \approx D_{active}$ and (ii) zero time spread within the ion bands. When an ion of mass $m + \Delta m$ approaches the ion selector, the time by which the ion's entry into deflector 1 is advanced ($\Delta m < 0$) or retarded ($\Delta m > 0$) with respect to that of m is $t_{entry}(m + \Delta m) = t_{entry}(m) + \Delta t_{dispersion}(\Delta m)$ where to the first order $\Delta t_{dispersion}(\Delta m) = \frac{1}{2}(\Delta m/m)t_{flight} \approx \frac{1}{2}(\Delta m/m)[L_1/v_z(m)]$ and L_1 is the distance from the ion source's exit grid to the ion selector's entry plane. If the ion's flight time through the ion selector is $\ll L_1/v_z(m)$, its exit time can be closely approximated by $t_{exit}(m + \Delta m) \approx t_{exit}(m) + \Delta t_{dispersion}(\Delta m)$. Substituting these quantities into Eqn (3) and, when simplifying, taking into account the fact that $p_x(m) = 0$ yields

$$p_x(m + \Delta m) = \frac{4q}{d}V_{gate}\Delta t_{dispersion}(m) \approx \frac{\Delta m}{m}\frac{L_1}{d}\frac{2qV_{gate}}{v_z(m)} \qquad (5)$$

If L_2 is the distance from the center of the ion selector to the detector, $x_{detector}(m + \Delta m)$ is the transverse displacement of the deflected ion at the detector plane, and $p_z(m) \equiv mv_z(m)$, then $\tan\theta = p_x(m + \Delta m)/p_z(m) = p_x(m + \Delta m)/mv_z(m) = x_{detector(m + \Delta m)}/L_2$ where θ is the half-angle subtended at the center of the deflection assembly by the ion path to the detector. Setting $x_{detector}(m + \Delta m) = \frac{1}{2}D_{active} \approx \frac{1}{2}D_{effective}$, substituting for $p_x(m + \Delta m)$ from Eqn (5), and rearranging yields the following approximate expression for the resolving power of either a single-deflector gate or dual-deflector gate ion selector operated by dynamically reversing its electric field:

$$\frac{m}{\Delta m} \approx 2\frac{L_1 L_2}{dD_{effective}}\frac{V_{gate}}{V_{accel}} \qquad (6)$$

Since this equation does not take time spread within an ion band into account, it predicts an upper limit for the resolving power.

Operating a single deflector in a field-reversed mode is convenient because its switching action permits the selection window to be positioned anywhere along the mass to charge scale by changing only one parameter, viz. $t_{t-single}(m)$. The mass range Δm of the selection window can be varied over a limited range in accordance with Eqn (6) by varying V_{gate}. Both of these operations can be performed while viewing a spectrum in real time on an oscilloscope screen or a computer monitor. The spectra of substance-P ($m/z = 1348.6$) shown in Fig. 6 illustrate these operational features of the single deflector and give an indication of the resolving power that can be attained with this device in the field-reversed mode. The mass spectrum shown in Fig. 6(a) was recorded from 7 laser pulses with the ion selector turned off. To isolate an isotopic envelope as shown in Fig. 6(b)–6(d), V_{gate} was set at the low value of 100 V, and to shift the window from one group of isotopic peaks to another, $t_{t-single}(m)$ was simply increased or decreased by amounts corresponding to the short times separating the envelopes, viz. 50 ns for $[M + H]^+ \leftrightarrow [M + Na]^+$ and 40 ns for $[M + Na]^+ \leftrightarrow [M + K]^+$. Increasing V_{gate} to 250 V was sufficient under the MALDI conditions used to zoom the selection window down to an individual isotopomer within a given isotopic envelope (Fig. 6(e)–6(g)). Signals from the immediately adjacent isotope ions ($m \pm 1$) were reduced to less that 33% of the selected ion's signal in all cases. A small level of unresolved signal, which typically varies from one spectrum to the next (Fig. 6(e)–6(g)), is observed in the vicinity of the $m + 3$ and $m + 4$ isotopomers. We have not yet discovered what causes it. Assuming triangular peaks and superimposing triangular transmission curves on the three peaks in Fig. 6(e)–6(g) gives an average $m/\Delta m$ of 710 (FWHM). Assuming triangular peaks and superimposing triangular transmission curves on the spectra in Fig. 6(e)–6(g) gives an average $m/\Delta m$ of approximately 710 (FWHM). In order to achieve this resolving power it is paramount that the exit plane of the ion source and the entrance plane of the ion selector be aligned as perpendicular to the flight axis as possible. Once properly aligned, operation of the ion selector in the single-deflector mode is very robust with respect to laser fluence. The latter can be increased well above threshold without increasing V_{gate} to maintain ion transmission. This feature could be of considerable advantage in PSD experiments.

As in the case of the single deflector, mass selection and mass resolving power can be independently varied with a dual deflector. For any given Δt_d, the position of the selection window along the mass to charge scale can be
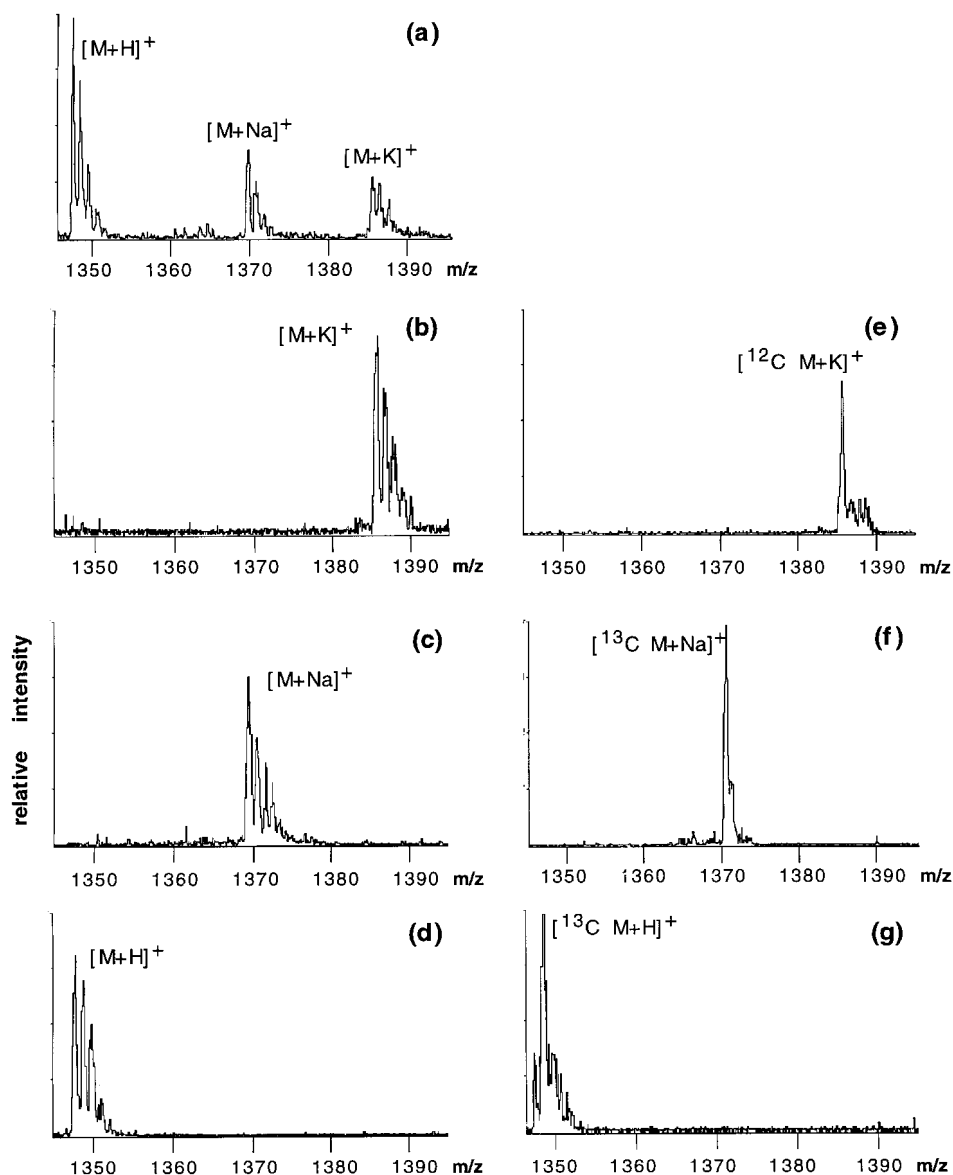
Figure 6. Single-deflector mass spectra (7–8 laser pulses per spectrum) of the salt-laden sample of substance-P showing the m/z region spanning $[M + H]^+$, $[M + Na]^+$ and $[M + K]^+$. (a) Both deflectors off (electrodes grounded). (b) Isolated $[M + K]^+$: $t_{t\text{-}single} = 7.130\ \mu s$, $V_{gate} = 100\ V$. (c) Isolated $[M + Na]^+$: $t_{t\text{-}single} = 7.090\ \mu s$, $V_{gate} = 100\ V$. (d) Isolated $[M + H]^+$: $t_{t\text{-}single} = 7.040\ \mu s$, $V_{gate} = 100\ V$. (e) Isolated $[^{12}CM + K]^+$: $t_{t\text{-}single} = 7.131\ \mu s$, $V_{gate} = 250\ V$. (f) Isolated $[^{13}CM + Na]^+$: $t_{t\text{-}single} = 7.091\ \mu s$, $V_{gate} = 250\ V$. (g) Isolated $[^{13}CM + H]^+$: $t_{t\text{-}single} = 7.040\ \mu s$, $V_{gate} = 250\ V$. Delayed extraction conditions: pulse = 2.066 kV, 2nd acceleration stage = 8.007 kV, delay = 2.4 μs.

selected by varying the trigger time $t_{t\text{-}dual}(m)$ exactly as it is done with a single deflector. By contrast, the dual deflector's resolving power is changed by varying Δt_d instead of V_{gate}. Increasing Δt_d from a minimum value approximately equal to the ion's transit time between the deflector centers, i.e. $g/v_z(m)$, seamlessly zooms the mass range of the dual deflector's selection window from approximately one mass unit to essentially any size desired. In this respect, the dual deflector is more versatile to operate in the field-reversal mode than the single deflector. Both positioning and sizing the selection window can be monitored in real time with an oscilloscope or a computer.

In order to achieve high resolution with the dual deflector, we found it necessary to adjust the laser fluence as close as possible to the threshold for ion desorption. With our current configuration, we observe losses in ion transmission of about 20%. We attribute most of this decrease to divergence of the ions within the beam. Because the aspect ratio (deflector width:deflector separation) of the wire strips we use as electrodes in our ion deflectors is greater than 1, the device's ion transmission will decrease as the cosine of the angle of incidence (defined with respect to the deflector's normal). It might be possible to increase the ion selector's transmission by focusing the ions into a parallel beam normally incident on the gate structure; however, any gain from doing this would have to be weighted against concomitant losses in resolution.

The mass spectra of substance-P shown in Figs 7 and 8 reflect the operating features and performance characteristics of our ion selector in the dual-deflector mode. Figure 7(a) shows the mass spectrum of substance-P with the ion selector turned off. With $\Delta t_d = 300\ ns$, changing the settings

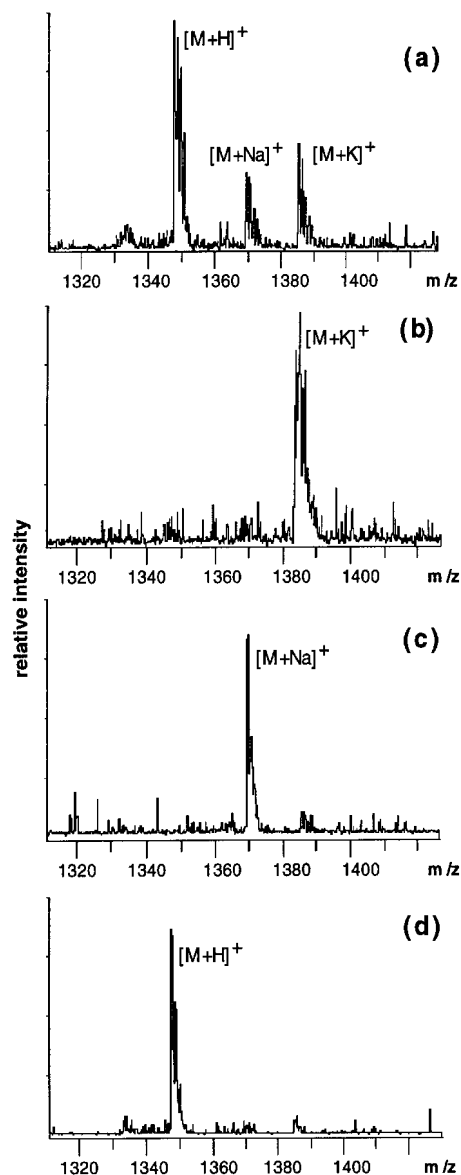**Figure 7.** Dual-deflector mass spectra (10 laser pulses per spectrum) of the salt-laden sample of substance-P showing the m/z region spanning $[M + H]^+$, $[M + Na]^+$ and $[M + K]^+$. (a) Both deflectors off. (b) Isolated $[M + K]^+$: $t_{t-dual} = 6.975$ µs, $\Delta t_d = 300$ ns, $V_{gate} = 425$ V. (c) Isolated $[M + Na]^+$: $t_{t-dual} = 6.935$ µs, $\Delta t_d = 300$ ns, $V_{gate} = 425$ V. (d) Isolated $[M + H]^+$: $t_{t-dual} = 6.875$ µs, $\Delta t_d = 300$ ns, $V_{gate} = 425$ V. Delayed extraction conditions: pulse = 2.8 kV, 2nd acceleration stage = 8.0 kV, delay = 2.8 µs.

of $t_{t-dual}(m)$ to the values indicated in the figure caption shifted the ion selector's mass window from one isotopic envelope to another as seen in Fig. 7(b)–7(d); the differences between the $t_{t-dual}(m)$ values correspond to the time intervals separating the ion envelopes as they arrive at the selector. Figure 8(a) shows a spectrum of the $[M + H]^+$ ions of substance-P in which the isotopic peaks are fully resolved at the baseline. Recording high resolution mass spectra under the conditions indicated in the figure caption was hindered by interferences either from the gate's fringe fields or stray fields from some, as yet unidentified source. Therefore, the spectra shown in Fig. 8 were produced from single laser pulses; this is reflected by variation in the isotopic pattern of each spectrum from the theoretical distribution for substance-P. The spectra shown in Fig. 8 are
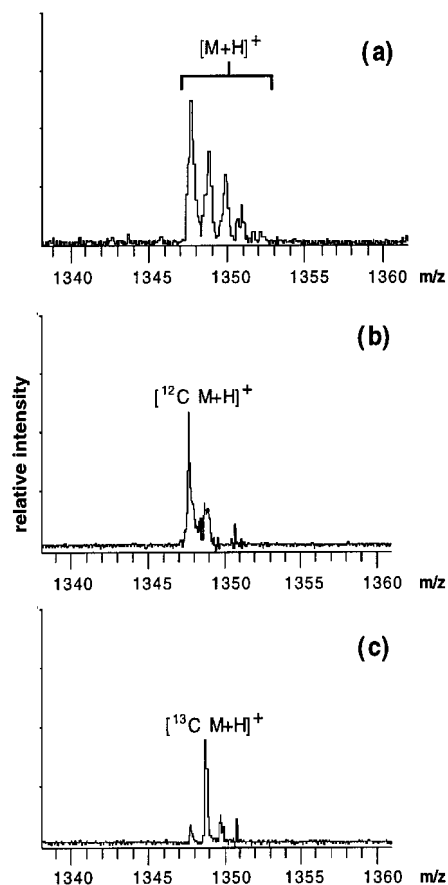
Figure 8. Dual-deflector mass spectra (1 laser pulse per spectrum) of the salt-laden sample of substance-P showing the m/z region in the vicinity of $[M + H]^+$. (a) Expanded view showing baseline resolution: $t_{t-dual} = 6.875$ µs, $\Delta t_d = 300$ ns, $V_{gate} = 425$ V. (b) Isolated $[^{12}CM + H]^+$; $t_{t-dual} = 6.875$ µs, $\Delta t_d = 280$ ns, $V_{gate} = 425$ V. (c) Isolated $[^{13}CM + H]^+$: $t_{t-dual} = 6.878$ µs, $\Delta t_d = 280$ ns, $V_{gate} = 425$ V. Delayed extraction conditions: pulse = 2.8 kV, 2nd acceleration stage = 8.0 kV, delay = 2.8 µs. The peak at m/z 1355 in panels (b) and (c) is a noise spike.

typical of those recorded with this compound. Leaving $t_{t-dual}(m)$ fixed at 6.875 µs but changing Δt_d from 300 ns to 280 ns zoomed the selector's time window in on the ^{12}C ions of the protonated molecule (Fig. 8(b)). Signal from the ^{13}C-isotope ions is still observed, but its strength relative to the ^{12}C-isotope ions is only 33% of what it was in Fig. 8(a). The selection window was shifted to the first ^{13}C isotope (Fig. 8(c)) by keeping Δt_d set at 280 ns but increasing $t_{t-dual}(m)$ by 3 ns, which agrees reasonably with the calculated time (1.9 ns) separating the ^{12}C and ^{13}C ions at the entrance to the ion selector. The heights of the first and third peaks in the isotopic group are approximately 13% and 20% respectively of height of the large middle peak. Superimposing a triangular curve on the three peaks in Fig. 8(c) gives a window for ion transmission of about 1.2 u (~2.2 ns) (FWHM), which corresponds to an $m/\Delta m$ of approximately 1100 (FWHM).

The mass spectra of PEG 6000 shown in Fig. 9(a) and 9(b) were produced by increasing L_1, the distance between the ion source and the gate (c in Fig. 1), from 200 mm to 900 mm, changing the DE-focusing, decreasing V_{accel} from 10.8 kV to 10.04 kV, and increasing V_{gate} from 425 V to 450 V. These changes enabled us to isolate the molecular
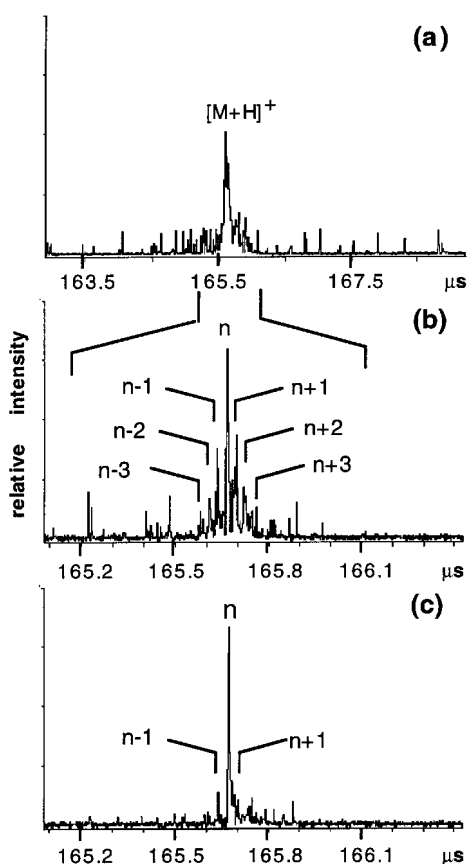
Figure 9. Dual-deflector mass spectra (10 laser pulses per spectrum) of PEG 6000 showing region in the vicinity of m/z 6,000. (a) Isolated $[M + H]^+$: $t_{t\text{-}dual} = 48.158$ μs, $\Delta t_d = 834$ ns, $V_{gate} = 425$ V; delayed extraction conditions: pulse = 1.04 kV, 2nd acceleration stage = 9.0 kV, delay = 1.25 μs. (b) Expanded view of isolated $[M + H]^+$ showing near baseline resolution; the peaks are labeled relative to the ^{13}C-number n of the base peak. (c) Isolated base peak $[^{13}C_nM + H]^+$: $t_{t\text{-}dual} = 48.158$ μs, $\Delta t_d = 832$ ns, $V_{gate} = 450$ V; delayed extraction conditions: pulse = 1.04 kV, 2nd acceleration stage = 9.0 kV, delay = 1.75 μs.

ion of one of the polymeric components in the vicinity of m/z 6000 with our dual deflector (Fig. 9(a)). The increased distance between the ion source and gate also reduced the interferences due to fringe or stray fields and, consequently, enabled us to record ions produced from 10 laser pulses without losing appreciable resolution (Fig. 9(b)). By changing the delay for ion extraction from 1.25 μs to 1.75 μs, increasing V_{gate} from 425 V to 450 V, and reducing Δt_d by 2 ns, we succeeded in improving the ion selector's resolution enough to isolate a single isotopomer at $\sim m/z$ 6000 (Fig. 9(c)). The calculated time between adjacent isotopomers of PEG 6000 at the entrance of the ion selector is 4.2 ns under the conditions indicated in Fig. 9. Assuming a triangular transfer function through the ion selector (as was done for substance-P spectra in Figs 6(e)–(g) and 8(c)), the spectrum shown in Fig. 9(c) corresponds to a transmission window of about 1.14 u ($\sim$4.8 ns), which converts to an $m/\Delta m$ of about 5200.

Substituting the values for the resolving powers obtained in the various modes of operation into the left side of Eqn (6) and solving for the effective diameter of the detector yields $D_{effective} \approx 32$ mm ($\sim$1.3 D_{active}), 33 mm (1.3 D_{active}), and 34 mm (1.4 D_{active}) for single-deflector substance-P, dual-deflector substance-P, and dual-deflector PEG 6000 respectively. These values are remarkably consistent. In

relation to the active diameter of the detector (25 mm), a range of 32–34 mm for $D_{effective}$ implies that half or more of the ions reaching the detector are within a cross-section less than or equal to 10 mm (i.e. $\leq 0.4 \, D_{active}$). Unless the actual beam size is substantially less than indicated by this reasoning, which is difficult to imagine, the resolving powers implicit in Figs 6(e)–(g), 8(c) and 9(c) should be close to the upper limits predicted in each case by Eqn (6). If this is so, the time spread within an ion band entering the ion selector should be close to the zero limit, i.e. $\ll \Delta t_{dispersion}(\Delta m)$. Regardless of whether this is in fact the case or not, using a dynamically operated ion selector together with delayed ion extraction to achieve mass resolving powers of 710 (single deflector) and 1100 (dual deflector) at $\sim m/z$ 1350 (in a mere 200 mm of flight) and 5200 (dual deflector) at $\sim m/z$ 6000 (in 900 mm of flight) suggests that mass dispersion at the entrance to an ion gating system does not impose the limitation on mass selectivity that Cotter[25] predicted.

In summary, we have created a new design and dynamic mode of operation for a combined single- and dual-deflector ion gate. The assembly is simple to construct. Care must be taken to align it as perpendicular to the flight axis of the instrument as possible. In conjunction with MALDI-MS, the single deflector's resolving power and transmission are robust with respect to laser fluence, i.e. they remain high even when the fluence is raised well above threshold. This operational feature should be particularly advantageous in PSD experiments. Operating the ion selector in the dual-deflector mode offers more versatility in locating and sizing the selection window, but in order to achieve high resolving power in this mode when performing MALDI-MS, the laser fluence must be kept near threshold. During the initial experiments with our prototype device, we succeeded in isolating single isotopomers of 10 keV ions up to m/z 6000 in the dual-deflector mode. A high resolution ion selection capability of this sort should increase both the number of PSD MALDI experiments that are possible and the amount of information that is obtainable from any given experiment.

Acknowledgements

REFERENCES

1. M. Karas and F. Hillenkamp, *Anal. Chem.* **60,** 2299 (1988).
2. K. Tanaka, H. Waki, Y. Ido, S. Akita, Y. Yoshida and T. Yoshida, *Rapid Commun. Mass Spectrom.* **2,** 151 (1988).
3. R. Kaufmann, B. Spengler and F. Lützenkirchen, *Rapid Commun. Mass Spectrom.* **7,** 902 (1993).
4. K. Schey, R. G. Cooks, R. Grix and H. Wollnik, *Int. J. Mass Spectrom. Ion Processes* **77,** 49 (1987).
5. K.-D. Rinnen, D. A. V. Kliner, R. S. Blake and R. N. Zare, *Rev. Sci. Instrum.* **60,** 717 (1989).
6. K. LaiHing, P. Y. Cheng, T. G. Taylor, K. F. Willey, M. Peschke and M. A. Duncan, *Anal. Chem.* **61,** 1458 (1989).
7. C. Brechignac, P. Cahuzac, J. Leygnier and J. Weiner, *J. Chem. Phys.* **90,** 1492 (1989).
8. D. R. Jardine, J. Morgan, D. S. Alderdice and P. J. Derrick, *Org. Mass Spectrom.* **27,** 1077 (1992).

9. R. E. Williams, L. Fang and N. R. Zare, *Int. J. Mass Spectrom. Ion Processes* **123,** 233 (1993).
10. T. J. Cornish and R. J. Cotter, *Anal. Chem.* **65,** 1043 (1993).
11. R. Weinkauf, K. Walter, C. Weickhardt, U. Boesl and E. W. Schlag, *Z. Naturforsch., A* **44,** 1219 (1989).
12. M. M. Cordero, T. J. Cornish, R. J. Cotter and I. A. Lys, *Rapid Commun. Mass Spectrom.* **9,** 1356 (1995).
13. P. R. Vlasak, D. J. Beussman, M. R. Davenport and C. G. Enke, *Rev. Sci. Instrum.* **67,** 68 (1996).
14. L. B. Loeb, *Basic Processes of Gaseous Electronics*, University of California, Berkeley, Berkeley (1961).
15. A. M. Cravath, *Phys. Rev.* **33,** 605 (1929).
16. N. E. Bradbury, *Phys. Rev.* **44,** 883 (1933).
17. R. Kaufmann, D. Kirsch and B. Spengler, *Int. J. Mass Spectrom. Ion Processes* **131,** 355 (1994).
18. T. Cornish and R. J. Cotter, *Rapid Commun. Mass Spectrom.* **6,** 242 (1992).
19. T. J. Cornish and R. J. Cotter, *Org. Mass Spectrom.* **28,** 1129 (1993).
20. T. J. Cornish and R. J. Cotter, *Rapid Commun. Mass Spectrom.* **7,** 1037 (1993).
21. F. H. Strobel, L. M. Preston, K. S. Washburn and D. H. Russell, *Anal. Chem.* **64,** 754 (1992).
22. E. Clayton and R. H. Bateman, *Rapid Commun. Mass Spectrom.* **6,** 719 (1992).
23. R. J. Cotter, T. J. Cornish and B. Musselman, *Rapid Commun. Mass Spectrom.* **8,** 339 (1994).
24. R. H. Bateman, M. R. Green, G. Scott and E. Clayton, *Rapid Commun. Mass Spectrom.* **9,** 1227 (1995).
25. R. J. Cotter, *Time-of-Flight Mass Spectrometry*, American Chemical Society, Washington, DC (1997).
26. W. C. Wiley and I. H. McLaren, *Rev. Sci. Instrum.* **26,** 1150 (1955).
27. H. Haberland, H. Kornmeier, C. Ludewigt and A. Risch, *Rev. Sci. Instrum.* **62,** 2368 (1991).
28. C. W. Stoermer, S. Gilb, J. Friedrich, D. Schooss and M. M. Kappes, *Rev. Sci. Instrum.* **69,** 1661 (1998).
29. M. Vestal, P. Juhasz, W. Hines and S. Martin, *An improved delayed extraction MALDI-TOF for PSD and CID*, Presented at the 46th ASMS Conf. Mass Spectrom. Allied Topics, Orlando, Florida (1998).
30. R. S. Brown and J. J. Lennon, *Anal. Chem.* **67,** 1998 (1995).
31. M. L. Vestal, P. Juhasz and S. A. Martin, *Rapid Commun. Mass Spectrom.* **9,** 1044 (1995).
32. C. M. Turner and S. D. Bloom, *Rev. Sci. Instrum.* **29,** 480 (1958).
33. T. K. Fowler and W. M. Good, *Nucl. Instrum. Methods* **7,** 245 (1960).